Traceable Multifunctional Micellar Nanocarriers for Cancer-Targeted Co-delivery of MDR-1 siRNA and Doxorubicin

Xiao-Bing Xiong[†] and Afsaneh Lavasanifar[†,‡,*]

[†]Faculty of Pharmacy and Pharmaceutical Sciences, [‡]Department of Chemical & Materials Engineering, Faculty of Engineering, University of Alberta, Edmonton, AB, Canada

ABSTRACT In this article we report on the development of polymeric micelles that can integrate multiple functions in one system, including the capability to accommodate a combination of therapeutic entities with different physicochemical properties (*i.e.*, siRNA and doxorubicin; DOX), passive and active cancer targeting, cell membrane translocation, and pH-triggered drug release. A micellar system was constructed from degradable poly(ethylene oxide)-*block*-poly(ε-caprolactone) (PEO-*b*-PCL) block copolymers with functional groups on both blocks. The functional group on the PCL block was used to incorporate short polyamines for complexation with siRNA or to chemically conjugate DOX *via* a pH-sensitive hydrazone linkage. A virus mimetic shell was conferred by attaching two ligands, *i.e.*, the integrin $\alpha v\beta 3$-specific ligand (RGD4C) for active cancer targeting and the cell-penetrating peptide TAT for membrane activity. This system was used to improve the efficacy of DOX in multidrug-resistant MDA-MB-435 human tumor models that overexpress P-glycoprotein (P-gp), by simultaneous intracellular delivery of DOX and siRNA against P-gp expression. The carrier was tagged with near-infrared fluorescent imaging probes to provide a means to follow the fate of the system *in vivo* upon intravenous administration. Dy677-labeled siRNA was also used to assess the *in vivo* stability of the siRNA carrier. This multifunctional polymeric micellar system was shown to be capable of DOX and siRNA delivery to their intracellular targets, leading to the inhibition of P-gp-mediated DOX resistance *in vitro* and targeting of $\alpha v\beta 3$-positive tumors *in vivo*.

KEYWORDS: polymeric micelles · cancer · multidrug resistance · siRNA · doxorubicin

Cancer is one of the major causes of mortality and morbidity in the world, and the incidence of cancer continues to increase. Chemotherapy is the treatment of choice in many cancers; however, its success has been limited, mostly because of systemic toxicity and the emergence of multidrug resistance (MDR). Anticancer drug toxicity is mainly due to the nonspecific distribution of chemotherapeutics in a biological system, leading to the exposure of normal tissues to the toxic effects of these drugs. Various nanocarrier platforms have been developed that can provide targeting of anticancer drugs to tumor tissue by taking advantage of the enhanced permeation and retention (EPR) effect in the tumor site. Further functionalization of the surface of the nanocarriers allows for enhanced recognition and uptake of the nanocarrier by cancer cells.[1−5]

Multidrug resistance to many conventional chemotherapeutic agents, including anthracyclines and taxanes, is commonly associated with cancer cell overexpression of drug transporter proteins such as P-glycoprotein (P-gp), which is encoded by the mdr1 gene.[6,7] Considerable efforts have been devoted to the development of specific small molecules that can inhibit the function of P-gp in order to sensitize tumor cells to conventional chemotherapeutics.[8] Despite this effort, no P-gp inhibitor has been approved for clinic use. This is mainly due to the nonspecific action of P-gp inhibitors on other molecular targets and/or their nonselectivity for tumorogenic P-gp, leading to intolerable toxicity by the P-gp inhibitor itself or by the anticancer drug upon co-administration with the P-gp inhibitor.[9] RNA interference (RNAi) technology mediated by small interfering RNA (siRNA) results in a potent post-transcriptional gene silencing. This strategy may be used to inhibit the expression (rather than function) of P-gp with high specificity and low off-target effect.[10−12] However, delivery of siRNA to tumorogenic P-gp upon systemic administration remains a major challenge. The delivery system for tumor-targeted siRNA delivery upon systemic administration should be designed to overcome hurdles such as poor stability, low cellular uptake, and rapid clearance of siRNA from the circulation. Nanoparticle platforms that can provide efficient delivery of siRNA and anticancer drugs to tumor site upon systemic administration are emerging as a promising

* Address correspondence to alavasanifar@pharmacy.ualberta.ca.

Received for review April 13, 2011 and accepted May 31, 2011.

Published online May 31, 2011
10.1021/nn2013707

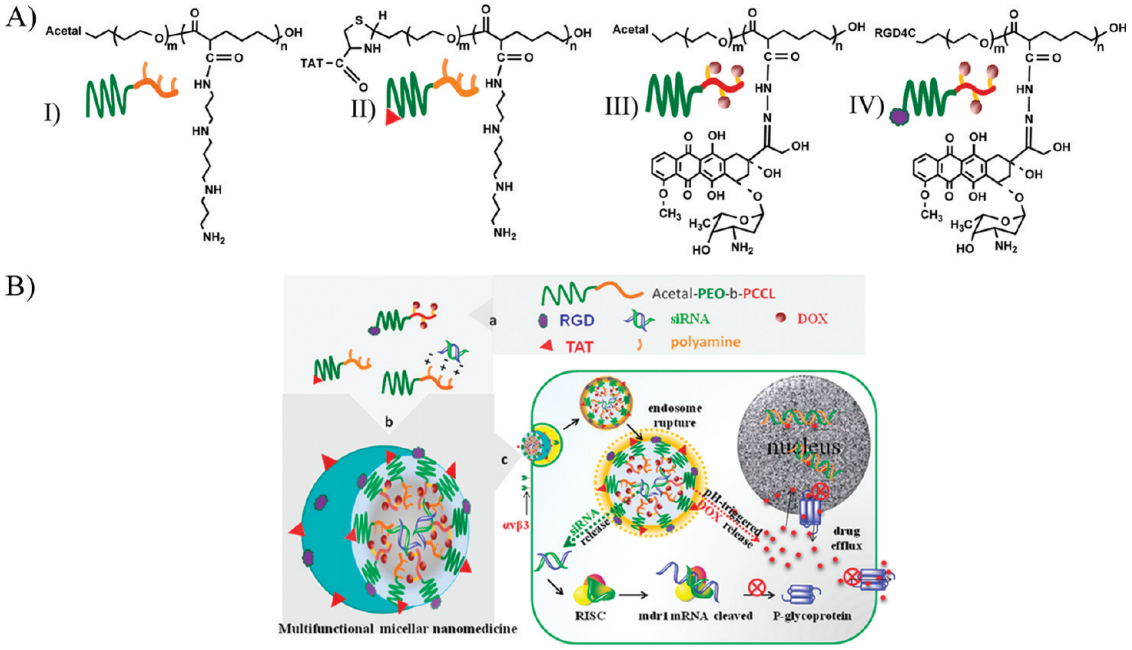

Figure 1. (A) Schematic illustration of acetal- and TAT-PEO-*b*-P(CL-g-SP) (I and II) and acetal- and RGD4C-PEO-*b*-P(CL-Hyd-DOX) (III and IV). (B) Rational design of a multifunctional micellar nanomedicine for targeted co-delivery of siRNA and DOX to overcome multidrug resistance. (a) Chemical structure of functionalized copolymers with ligands at the end of the PEO block and conjugated moieties on the PCL block. (b) Assembly of multifunctional micelles with DOX and siRNA in the micellar core and RGD and/or TAT on the micellar shell. (c) Schematic diagram showing the proposed model for the intracellular processing of targeted micelles in MDR cancer cells after receptor-mediated endocytosis, leading to cytoplasmic siRNA delivery followed by P-gp down-regulation on the cellular and nuclear membrane and endosomal DOX release, followed by DOX nuclear accumulation.

way to improve cancer treatment.[13−16] A better therapeutic effect in MDR tumors by co-localization of anticancer drugs and siRNA against P-gp in the same cancer cell can be envisioned.[17−21]

Polymeric micelles self-assembled from biodegradable amphiphilic block copolymers represent one of the potential nanodelivery systems for targeted co-delivery of siRNA and anticancer drugs.[22] Among different micelle-forming amphiphilic block copolymers, those composed of poly(ethylene oxide) (PEO) and polyesters such as poly(ε-caprolactone) (PCL) and poly(lactic acid) (PLA) have attracted much attention, as they are FDA-approved biomaterials used in pharmaceutical formulations or medical devices.[23−25] In previous papers, we reported on the development of cancer-targeted PEO-*b*-PCL micelles for intracellular DOX delivery. The multifunctional micelles with targeting ligands (RGD4C) on the micellar shell and hydrazone-bonded doxorubicin (DOX) in the micellar core demonstrated better activity than free DOX in drug-sensitive cancer cells expressing integrin αvβ3, but were not effective in overcoming P-gp-mediated DOX resistance.[26] We have also designed PEO-*b*-PCL micelles with grafted polyamine in the PCL section for siRNA delivery to down-regulate P-gp expression in MDR cancer cells.[27] To introduce cancer targeting and also increase the transfection efficiency of this system for siRNA delivery, virus-mimetic polymeric micelles with two functional peptides (RGD4C and TAT) on their shell were developed. Decoration of polymeric micelles with RGD and TAT peptides led to effective P-gp down-regulation and reversal of DOX resistance in MDR cells.[28] The goal of the present study was to combine the two optimized siRNA and DOX polymeric micellar delivery systems and develop an integrated nanodelivery system for efficient and targeted co-delivery of DOX and siRNA against P-gp expression for overcoming MDR. In this context, traceable micellar systems based on PEO-*b*-PCL copolymers, containing either polyamine (Figure 1A, I) or DOX attached through hydrazone linkage (Figure 1A, III) on PCL were developed. The shell-forming blocks were also modified with TAT (Figure 1A, II) and RGD4C peptide (Figure 1A, IV), respectively. The final micellar formulation was achieved through mixing of plain or peptide-modified PEO-*b*-P(CL-g-SP)/siRNA and PEO-*b*-P(CL-Hyd-DOX) block copolymers (Figure 1B, panel a and b). A near-infrared fluorophore (NIRF) was chemically conjugated to the polyamine side chain, or fluorescently labeled siRNA was used to provide a means for following the fate of carrier as well as the incorporated siRNA *in vivo* (Figure 6A). This micellar system was expected to (i) be recognized by αvβ3 integrins over-expressed on cancer cell surface, (ii) be taken up specifically by those cells through receptor-mediated endocytosis, (iii) provide acidic pH-triggered release of free DOX in endosomes, and (iv) provide endosomal rupture and cytoplasmic siRNA delivery by spermine

TABLE 1. Preparation of RGD- and/or TAT-Functionalized Micelles for Co-delivery of siRNA and DOX[a]

micelles	composition (weight ratio)[b]	particle size (nm)[c]	zeta-potential (mV)
NON-micelles	I:III/siRNA (16:32:1)	93.4 ± 3.4	1.89 ± 0.24
RGD-micelles	I:IV/siRNA (16:32:1)	108.2 ± 4.2	2.81 ± 0.32
TAT-micelles	I:III:II/siRNA (8:32:8:1)	100.5 ± 4.8	6.15 ± 0.19
RGD/TAT-micelles	I:IV:II/siRNA (8:32:8:1)	103.4 ± 5.1	4.23 ± 0.51

[a] Chemical structure of polymers is shown in Figure 1A. [b] (I) acetal-PEO-*b*-P(CL-g-SP), (II) TAT-PEO-*b*-P(CL-g-SP), (III) acetal-PEO-*b*-P(CL-Hyd-DOX), (IV) RGD4C-PEO-*b*-P(CL-Hyd-DOX). [c] Average measured by dynamic light scattering technique.

and the TAT peptide. Efficient cytoplasmic delivery of siRNA and DOX by this polymeric micellar system was expected to down-regulate P-gp expression on cell and nuclear membranes, allowing cytoplasmic and nuclear accumulation of released DOX and resulting in DOX toxicity in MDR cells (Figure 1B).

RESULTS

Polymer Synthesis. The copolymers acetal-PEO-*b*-poly(α-carboxyl-ε-caprolactone) (acetal-PEO-*b*-PCCL) with pendant hydrazone-bonded DOX, spermine (SP), or *N*,*N*-dimethyldipropylenetriamine (DP) on the PCL block, *i.e.*, acetal-PEO-*b*-P(CL-Hyd-DOX), acetal-PEO-*b*-P(CL-g-SP), and acetal-PEO-*b*-P(CL-g-DP), respectively, were synthesized and characterized as reported.[26,28] The substitution level (molar ratio of the pendant groups to α-carboxyl-3-caprolactone units of the PCL block) was estimated at 30% for acetal-PEO-*b*-P(CL-Hyd-DOX), 53% for acetal-PEO-*b*-P(CL-g-SP), and 59% for acetal-PEO-*b*-P(CL-g-DP). Cy5.5 was further conjugated to the end of SP, and Cy5.5 conjugation efficiency was calculated to be ~1% (molar ratio of Cy5.5 to polymer).

Conjugation of peptide to the PEO end of the copolymers was performed by converting the acetal to an active aldehyde. Conjugation of RGD4C peptide to the PEO terminus of acetal-PEO-*b*-P(CL-Hyd-DOX) and acetal-PEO-*b*-P(CL-g-DP) was by Schiff base reaction, and conjugation of TAT to the acetal-PEO-*b*-P(CL-g-SP) was by formation of a thiazolidine ring between the cysteine and the aldehyde. The conjugation density (molar ratio of peptide to polymer) was calculated to be ~20% for RGD4C-PEO-*b*-P(CL-Hyd-DOX) and RGD4C-PEO-*b*-P(CL-g-DP) and ~18% for TAT-PEO-*b*-P(CL-g-SP).

Preparation and Characterization of NON- and RGD-Micelles for Co-delivery of siRNA and DOX and for *in Vivo* Imaging. The micellar co-delivery system was constructed from the synthesized functionalized PEO-*b*-PCL copolymers (Figure 1A). Table 1 summarizes the compositions, average diameters, and zeta-potentials of multifunctional micelles containing electrostatically bound siRNA and hydrazone-bound DOX. The resulting micelles have the same composition in the micellar core but have different moieties on the micellar shell. All the micellar formulations have a DOX loading content of ~6.0% (weight ratio of DOX to polymer). All the micelles have very similar average diameters (from 93 to 108 nm), suggesting that surface modification did not significantly change the particle size. However, modification of the micelles with positively charged TAT led to a slight increase of zeta-potential from 1.89 mV for NON-micelles to 6.15 mV for TAT-micelles and 4.23 mV for RGD/TAT-micelles. The peptide densities of RGD4C and TAT on the corresponding micelle surface are around 13.3% and 3.0% (molar ratio of peptide to polymer), respectively. NON- or RGD-micelles containing conjugated Cy5.5 or complexed Dy677-siRNA showed an average size of ~100 nm (data not shown).

The successful formation of mixed micelles upon mixing the two types of co-polymers was further demonstrated with acetal-micelles composed of acetal-PEO-*b*-P(CL-g-SP)/FAM-siRNA and acetal-PEO-*b*-P(CL-Hyd-DOX). Two-color flow cytometry analysis was used to confirm the formation of mixed micelles (Figure 2A). The acetal-PEO-*b*-PCL blank micelles were used as a negative control (Figure 2A-a), acetal-PEO-*b*-P(CL-g-SP)/FAM-siRNA micelles were green fluorescence positive (green area) (Figure 2A-b), and acetal-PEO-*b*-P(CL-Hyd-DOX) micelles were red fluorescence positive (Figure 2A-c). As expected, just one population of particles was observed for the resulting mixed micelles (both green and red fluorescence positive) (Figure 2A-d), suggesting that DOX and FAM-siRNA were simultaneously present in the same micelles. NON-micelles appeared to be discrete, round nanoparticles under AFM (Figure 2B-a). According to DLS data, NON-micelles containing both DOX and SP/FAM-siRNA in their core had a unimodal distribution and larger hydrodynamic diameter (93 nm) than acetal-PEO-*b*-P(CL-g-SP)/FAM-siRNA complex micelles (60 nm) (Figure 2B-b). The gel electrophoretic analysis showed that NON-micelles had a capacity to bind siRNA similar to that of acetal-PEO-*b*-P(CL-g-SP) micelles (Figure 2C). The pH-triggered DOX release from the mixed micelles was demonstrated by a fluorescence-dequenching experiment. DOX was effectively released from the micellar core under endosomal pH (5.0) so that an increasing DOX fluorescence intensity was observed over time (Figure 2D-a); however, DOX was retained in the micellar core at physiological pH 7.2, where its fluorescence remained quenched (Figure 2D-b).

Cellular Uptake. The two-color flow cytometry was used to quantify the cellular uptake of mixed micelles by MDA-MB-435/LCC6MDR1-resistant cells (Figure 3). Compared to NON-micelles, TAT- and RGD-micelles significantly increased cellular uptake of FAM-siRNA (Figure 3A and C) and DOX (Figure 3B and D), while a maximum 3-fold increase was achieved with RGD/TAT-micelles relative to NON-micelles. It is worth noting that, first, the same peptide-micelle led to a similar extent of increase in cellular uptake of FAM-siRNA and

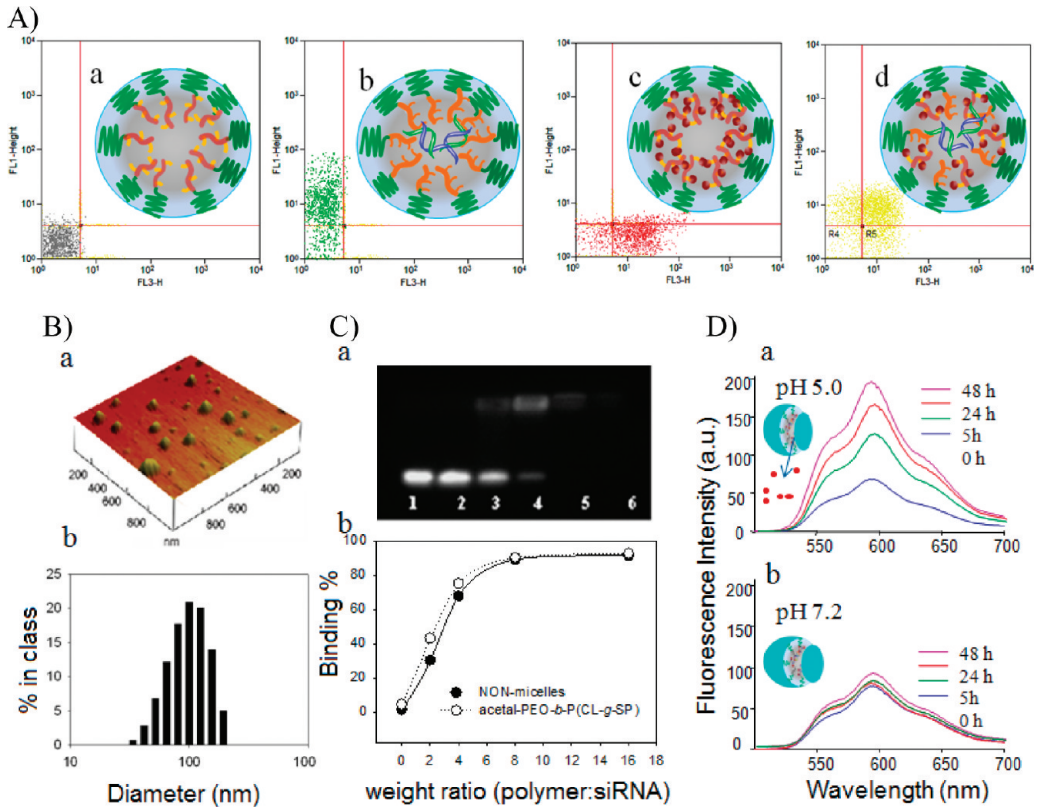

Figure 2. Characterization of multifunctional micelles with co-encapsulated siRNA and DOX. (A) Flow cytometry analysis of mixed micelles with complexed FAM-siRNA, conjugated DOX, or both FAM-siRNA and DOX in the core: (a) acetal-PEO-*b*-PCL/acetal-PEO-*b*-P(CL-g-SP) mixed micelles (negative control, black), (b) acetal-PEO-*b*-P(CL-g-SP)/siRNA micelles (green), (c) acetal-PEO-*b*-P(CL-Hyd-DOX) micelles (red), (d) mixed micelles containing conjugated DOX and complexed FAM-siRNA (yellow). (B) Particle size of NON-micelles was analyzed by (a) AFM and (b) DLS (Zetasizer). (C) Electrophoretic analysis of siRNA binding by NON-micelles prepared from acetal-PEO-*b*-P(CL-g-SP) or acetal-PEO-*b*-P(CL-Hyd-DOX). The gel results for the acetal-micelles are shown in (a), in which lane numbers correspond to micelles with different weight ratios of acetal-PEO-*b*-P(CL-Hyd-DOX)/acetal-PEO-*b*-P(CL-g-SP)/siRNA: (1) siRNA only, (2) 16:0:1, (3) 16:2:1, (4) 16:4:1, (5) 16:8:1, (6) 16:16:1. The densitometric analysis of the binding results for acetal-micelles and acetal-PEO-*b*-P(CL-g-SP) is shown in (b). (D) DOX release from NON-micelles under (a) pH 5.0 and (b) pH 7.2.

DOX compared to acetal-micelles. Second, the cellular uptake of RGD/TAT-micelles in the presence of an excess of free ligand (cRGDfK, 5 mM) was dramatically reduced, becoming essentially equivalent to that of TAT-micelles, pointing to the involvement of receptor-mediated endocytosis. These observations once again confirmed that the mixed micelles containing both siRNA and DOX in the micellar core, rather than separate micelle populations, were formed from these co-polymers.

Intracellular Distribution and Endosome Escape. The cellular uptake and intracellular distribution of the micellar nanodelivery system was further studied by confocal microscopy (Figure 4). After 1 h of incubation of TAT- and RGD-micelles with MDA-MB-435/LCC6MDR1 cells, increased intracellular DOX fluorescence (red) and FAM-siRNA fluorescence (green) were observed in the cytoplasm, while the strongest DOX and green fluorescence were found with cells incubated with RGD/TAT-micelles (Figure 4A). This observation was in line with our previous findings and data of flow cytometry studies (Figure 3).

To evaluate the mixed micelle capability of endosomal escape, the endolysosome compartment of the cells was stained with LysoTracker (green, red, or blue) after treatment with endosomolytic or non-endosomolytic micelles (Figure 4B). After 4 h incubation, acetal-PEO-*b*-P(CL-Hyd-DOX) micelles without endosomolytic polymer (*i.e.*, acetal-PEO-b-P(CL-g-SP)) were almost completely entrapped in endolysosomes, as indicated by the co-localization of red and green fluorescence (yellow area) (Figure 4B-a). Micelles of acetal-PEO-*b*-P(CL-g-SP) with complexed FAM-siRNA were able to cause lysis of the endosome membrane, leading to distribution of FAM-siRNA outside of the endolysosomes (Figure 4B-b), which is consistent with our previous observation.[27,28] As expected, mixed micelles composed of acetal-PEO-*b*-P(CL-Hyd-DOX) and endosomolytic acetal-PEO-*b*-P(CL-g-SP) caused endosome membrane lysis, leading to DOX escape from the endosomes (Figure 4B-c). Finally, mixed micelles of acetal-PEO-*b*-P(CL-Hyd-DOX) and acetal-PEO-*b*-P(CL-g-SP) containing conjugated DOX and complexed FAM-siRNA caused membrane lysis, leading to

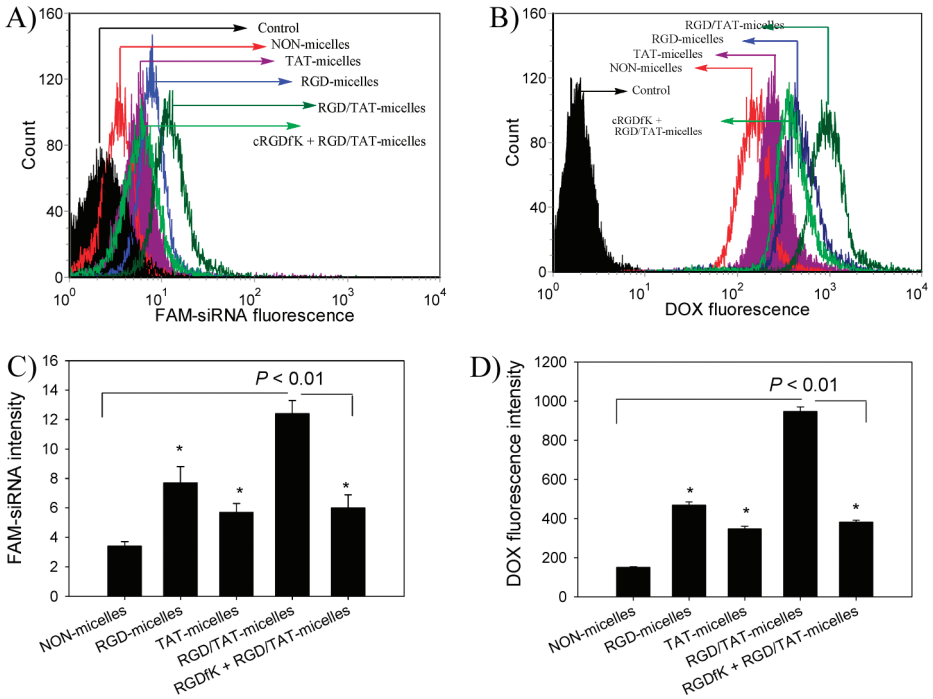

Figure 3. Cellular uptake of DOX and siRNA co-delivered by micelles with different surface moieties by flow cytometry after 1 h incubation. Flow cytometric histogram profiles of fluorescence intensity for cells treated with micelles containing FAM-siRNA (A) and hydrazone-bound DOX (B); the mean intensity of FAM-siRNA and DOX fluorescence from A and B is presented in C and D, respectively. The data are the mean ± standard error for $n = 3$. *$p < 0.05$ compared to NON-micelle.

both DOX (red) and FAM-siRNA (green) distribution outside of the endolysosomes (blue) (Figure 4B-d).

Intracellular DOX Accumulation and Cytotoxicity. Confocal microscopy was used to evaluate DOX accumulation in resistant cells after treatment with micellar co-delivery systems. Similar to our previous study, free DOX, which is the substrate of P-gp, demonstrated weak accumulation only in the cytoplasm of resistant cells (data not shown). Whereas treatment of resistant cells with micellar DOX-conjugates led to higher DOX accumulation in the cytoplasm of resistant cells, treatment with RGD-, TAT-, and RGD/TAT-micelles further increased intracellular accumulation of the micelles by enhancing cellular uptake. In particular, cells treated with RGD/TAT-micelles for co-delivery of mdr1 siRNA and DOX showed strong DOX fluorescence in the nucleus of resistant cells, as indicated by the green arrow in Figure 5A. The enhanced nuclear accumulation of DOX following co-delivery with mdr1 siRNA was also observed for RGD- and TAT-micelles, but to a lesser extent. In contrast, no nuclear DOX accumulation after incubation with RGD-, TAT-, or RGD/TAT-micelles containing DOX and scrambled siRNA after 72 h was observed.

The cytotoxicity of targeted micelles with mdr1 siRNA and DOX against MDA-MB-435/LCC6MDR1-resistant cells was investigated at a DOX concentration of 5 μg/mL (Figure 5B). As expected, targeted micelles formulated to deliver scrambled siRNA plus DOX were no more cytotoxic than free drug or targeted micelles without siRNA. Importantly, targeted micelles with mdr1 siRNA and bound DOX were significantly more cytotoxic than targeted micelles with scrambled siRNA and bound DOX or targeted micelles with bound DOX only. Notably, RGD/TAT-micelles with DOX and mdr1 siRNA demonstrated a maximum of ~70% of cell growth inhibition. This observation was consistent with our findings on the cell uptake and nuclear distribution of DOX when co-delivered with mdr1 siRNA in RGD/TAT-micelles.

***In Vivo* Optical Imaging Study.** RGD-functionalized micelles containing NIRF imaging probes were prepared for *in vivo* imaging (Figure 6A). Athymic mice bearing MDA-MB-435/LCC6MDR1-resistant tumors were used as the animal model. RGD- and NON-micelle-DOX-Cy5.5 were intravenously injected into these mice, and a significant tumor accumulation of RGD-micelles was observed 24 h after injection, indicating highly specific tumor targeting of RGD-micelles (Figure 6B). NON-micelles-DOX-Cy5.5 did not show obvious fluorescence in tumors, but showed high intensity of fluorescence in liver and kidney.

To test whether this system can effectively deliver complexed siRNA to the tumor, RGD- and NON-micelles/Dy677-siRNA were injected into athymic nude mice bearing MDA-MB-435/LCC6MDR1-resistant tumors, and *in vivo* optical imaging was performed. Similar to what has been observed for the labeled RGD-micelles themselves, a significant fluorescence of Dy677-siRNA was observed in tumors 24 h after

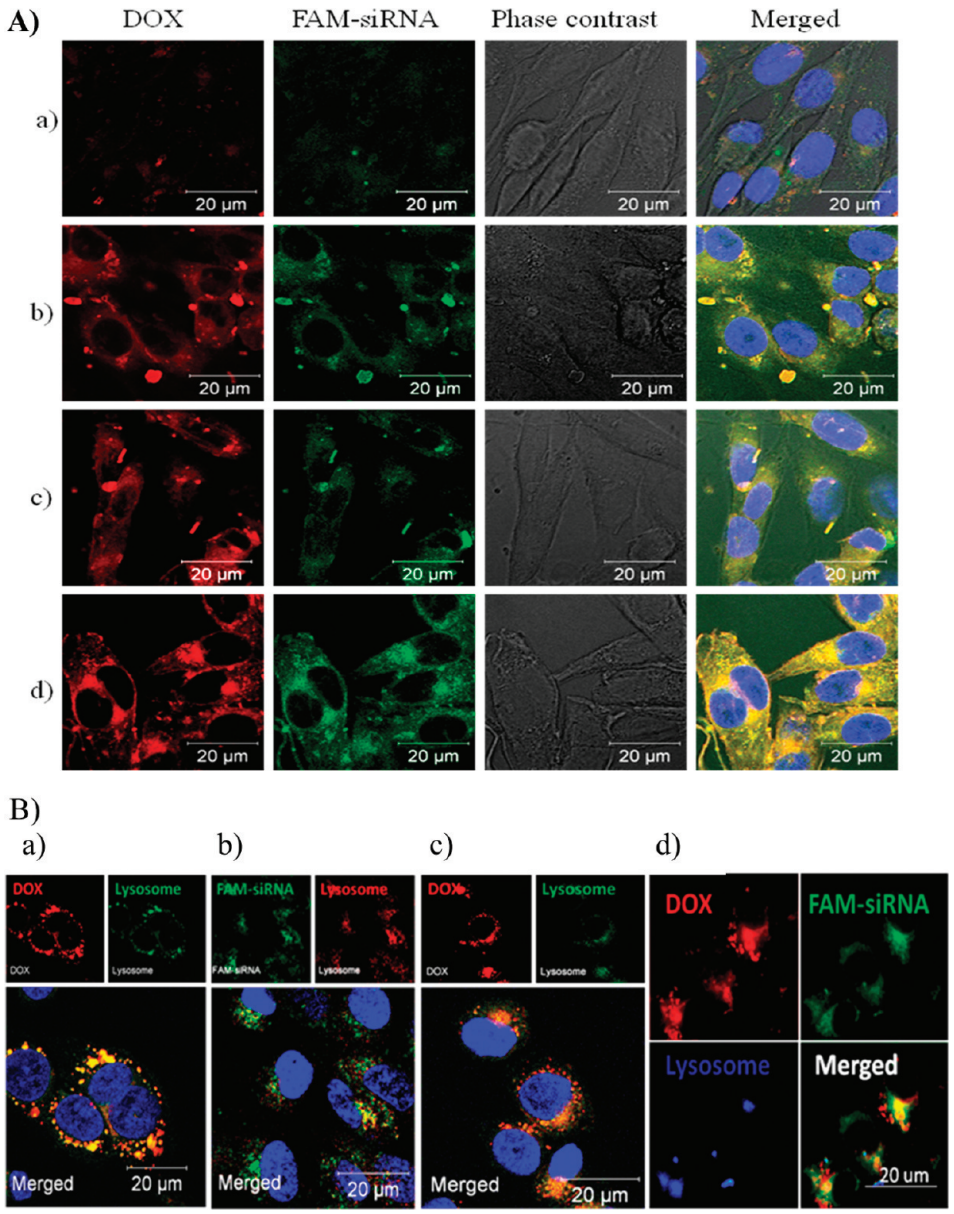

Figure 4. (A) Cellular uptake of DOX and FAM-siRNA delivered by micelles with different shell functionalization. MDA-MB-435/LCC6MDR1-resistant cells were incubated with (a) NON-micelles, (b) RGD-micelles, (c) TAT-micelles, and (d) RGD/TAT-micelles containing FAM-siRNA (200 nM) and DOX (5 ug/mL) for 1 h. (B) Intracellular distribution of various micelles in MDA-MB-435/LCC6MDR1-resistant cells after 4 h incubation. Cells were incubated with micelles composed of (a) acetal-PEO-*b*-P(CL-Hyd-DOX), (b) acetal-PEO-*b*-P(CL-g-SP)/FAM-siRNA (polymer/siRNA: 8:1), (c) acetal-PEO-*b*-P(CL-Hyd-DOX)/acetal-PEO-*b*-P(CL-g-SP) (weight ratio 1:2), and (d) acetal-PEO-*b*-P(CL-Hyd-DOX)/acetal-PEO-*b*-P(CL-g-SP)/FAM-siRNA (weight ratio 1:2). After 3.5 h, LysoTracker was added and incubated for another 0.5 h. The endolysosomes were stained by LysoTracker Green (green) for a and b, LysoTracker Red (red) for c, and LysoTracker Blue (blue) for d. Cell nuclei were stained with DAPI (blue) for a, b, and c.

injection, suggesting that these micelles can stably complex and protect siRNA in the micelle core and deliver the siRNA into tumor tissue, while NON-micelles/Dy677-siRNA did not show obvious fluorescence accumulation in the tumor (Figure 6C).

DISCUSSION

The main objective of this study was to develop a micellar nanodelivery system for effective co-delivery of siRNA and DOX, to improve the efficacy of systemic chemotherapy for treatment of MDR tumors. This system was based on a micellar carrier, which is structurally flexible enough to allow the integration of multiple functions into one technology. To our best knowledge, this is the first reported traceable multifunctional micellar system for integrating targeted delivery of siRNA and an anticancer drug through pH-triggered intracellular drug release for overcoming drug resistance in cancer.

P-gp overexpression is one of the major mechanisms of MDR in cancers. P-gp is also constitutively expressed in normal cells, such as capillary endothelial cells in the

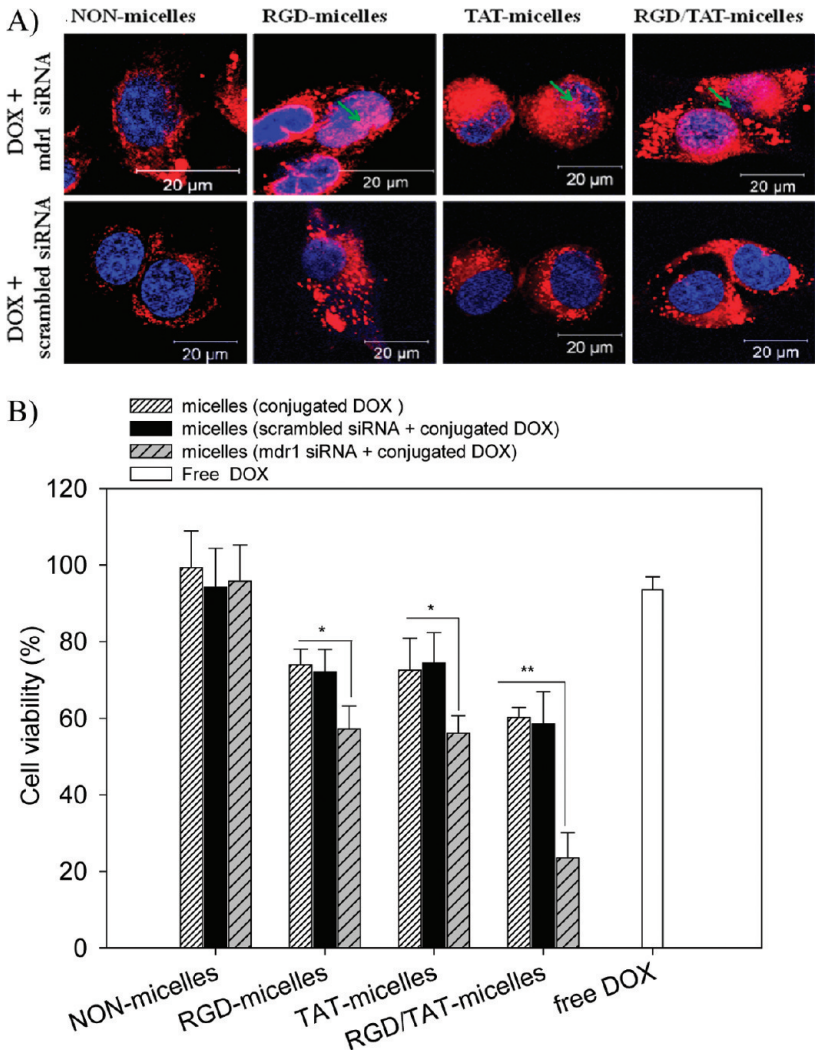

Figure 5. (A) DOX distribution in MDA-MB-435/LCC6MDR1-resistant cells after 72 h treatment with acetal-micelles, RGD-micelles, TAT-micelles, or RGD/TAT-micelles containing hydrazone-bound DOX (5 μg DOX equivalent/mL) and complexed mdr1 siRNA (100 nM). (B) Inhibition of cell growth of resistant cells in the presence of different formulations of complexed mdr1 siRNA (100 nM) and hydrazone-bound DOX (5 μg DOX equivalent/mL) after 72 h of incubation. Nontargeted micelles with hydrazone-bonded DOX (5 μg DOX equivalent/mL) and scrambled siRNA (100 nM) were used as a control. *$p < 0.05$, **$p < 0.01$, $n = 6–8$.

brain, and plays an important role in the physiological regulation of endogenous toxins and xenobiotics in the body. Therefore, it is important to deliver inhibitors of P-gp, specifically to tumorogenic P-gp. Further, for optimal synergy, the anticancer drugs that are both P-gp substrates and P-gp inhibitors, *i.e.*, siRNA in this case, may need to be spatially co-localized in the same population of tumor cells. The strategy of targeted co-delivery makes it possible to meet these challenges.

To date, various co-delivery systems have been formulated with the aim of delivering both siRNA and anticancer drugs to cancer cells to overcome MDR. For instance, co-delivery of mdr1 siRNA and paclitaxel by biotin-functionalized nanoparticles composed of PLGA and PEI demonstrated P-gp gene silencing *in vitro* and tumor drug resistance reversal *in vivo* in BALB/c mice bearing P-gp-overexpressing JC tumors.[13] Chen *et al.* developed a sigma-receptor targeted liposomal co-delivery system for DOX and siRNA and demonstrated its potential to overcome multidrug resistance.[15] More recently, mesoporous silica nanoparticles were engineered to deliver DOX and mdr1-siRNA to overcome MDR.[29]

We have reported on the development of RGD-functionalized micelles with DOX conjugated with a hydrazone linker that were able to enhance the efficacy of DOX in sensitive tumor models.[26] However, the released DOX in the cytoplasm was pumped out of the cells and failed to accumulate in the nucleus of P-gp-overexpressing DOX-resistant cells. Moreover, we have developed virus-mimetic micelles with complexed mdr1-siRNA capable of improving DOX cellular uptake, P-gp silencing, and overcoming resistance to free DOX.[26] The micellar system reported here has integrated these two designs in one single entity for targeted co-delivery of DOX and siRNA. The system

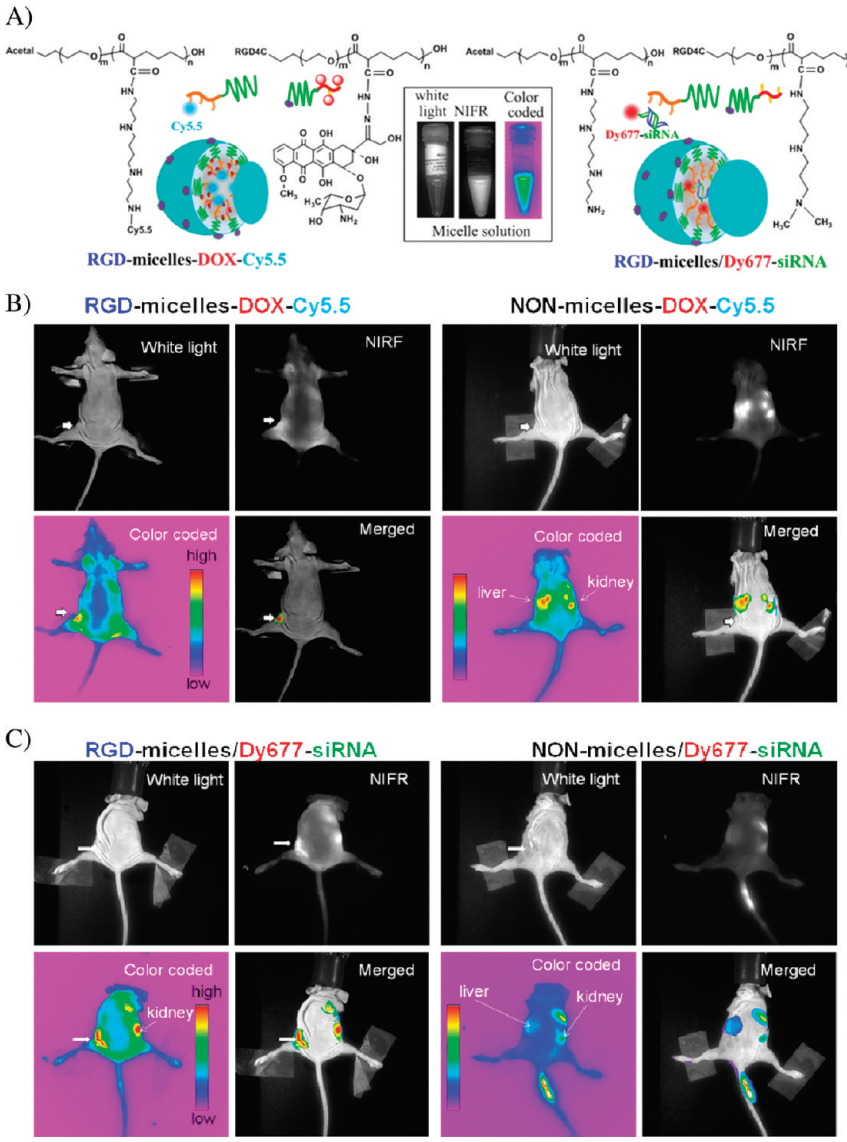

Figure 6. (A) Schematic illustration of polymer structures and assembled RGD-functionalized micelles containing NIRF imaging probes. The insets show images of one of those NIRF formulations. (B) Athymic nude mice bearing MDA-MB-435/LCC6MDR1-resistant tumors injected with RGD- and NON-micelles-DOX-Cy5.5. (C) Athymic nude mice bearing MDA-MB-435/LCC6MDR1-resistant tumors injected with RGD- and NON-micelles/Dy677-siRNA. MDA-MB-435/LCC6MDR1-resistant cells were transplanted subcutaneously into the right rear flanks of the mice, and tumor was approximately 0.1 cm^3 17 days after implant. The mice were imaged at 24 h after injection. The intensity of fluorescence is expressed by different colors, with pink reflecting the lowest intensity (background) and red reflecting the highest intensity. The tumor is indicated by the thick arrow.

was expected to show control over the localized release of the anticancer agent DOX, preferentially releasing DOX inside tumor cells due to endosomal pH-sensitive triggered release following uptake of the micellar carrier *via* integrin-mediated endocytosis through the RGD ligand. The virus-mimetic shell conferred by the dual-functional moieties, *i.e.*, integrin $\alpha v\beta 3$-targeted RGD for cell-specific recognition and cell penetration peptide TAT for efficient cell membrane translocation, was expected to enhance the delivery of siRNA to its cellular and intracellular targets (Figure 1). Targeted co-delivery of mdr1-siRNA was expected to enhance the delivery of DOX to its intracellular target in the cell nucleus through efficient inhibition of P-gp expression on the nuclear membrane, leading to resensitization of MDR cells to DOX. Finally, this system was expected to show a desirable pharmacokinetic profile for efficient tumor targeting of carrier and incorporated siRNA *in vivo* because of the stealth properties of the PEO shell, the presence of the tumor-targeting RGD ligand, and stable complexation of siRNA by the carrier. The validity of these hypotheses was tested in this study.

Characterization studies provided evidence for the formation of micelles with an appropriate size for tumor targeting by the EPR effect (around 100 nm), that were capable of incorporating DOX and siRNA in the same micellar entity (Figure 2A–C). The

integrated micelles have also shown acidic pH-triggered release of DOX from the micellar core (Figure 2D). The virus-mimetic shell containing the targeting moieties, RGD and TAT, was recognized by integrin $\alpha v\beta 3$-positive cancer cells, leading to facilitated cellular uptake of both micellar incorporated siRNA and DOX by those cells (Figures 3 and 4). The uptake of both siRNA and DOX was found to be enhanced with micelles with dual functionality compared to ones containing only RGD or TAT. These data were in agreement with our previous observation confirming the co-encapsulation of DOX and siRNA in the same micellar entities. Introduction of the TAT peptide to the micellar shell is expected to enhance the cellular internalization of micellar carriers in a nonspecific manner. The RGD peptide decoration was therefore used to introduce specificity for $\alpha v\beta 3$ integrins overexpressed on cancer cells for the carrier in addition to membrane activity, which was presented by the TAT peptide. Upon endocytosis, the polyamine moieties in the micelle core were able to rupture endosomes, perhaps by a "proton sponge effect", leading to the release of siRNA into the cytoplasm within 4 h incubation (Figure 4B-b). DOX, as part of acetal-PEO-P(CL-HYD-DOX), was localized in the endosomes (Figure 4B-a). This observation was consistent with our previous data.[26,28] However, DOX release in the cytoplasm was observed as part of the integrated micelles (Figure 4B-c). Interestingly, DOX and FAM-siRNA were only partly co-localized in the cytoplasm after 4 h incubation (Figure 4B-d), indicating the release of both entities in the cytoplasm upon collapse of the micelles in the endosomes. The SP portion of the polymer is suggested to cause the proton sponge effect, leading to endosomal rupture. This may account for a possible mechanism for the endosomal escape and cytoplasmic delivery of DOX in cleaved or conjugated form of the integrated micellar formulation. In addition, at acidic pH of the endosomes, free DOX may get trapped because of the protonation of its amine group. However, when given as part of the integrated micellar formulation, the buffering action of the polycation SP may lead to a reduction in the protonation of DOX, facilitating its diffusion out of the endosomes.

The conjugated DOX delivered by the multifunctional micelles bypassed cell membrane P-gp recognition and efflux particularly when delivered by RGD/TAT-micelles, but was unable to diffuse into the cell nucleus without the aid of mdr-1 siRNA (Figure 5A). Localization of DOX in the nucleus was observed only when mdr1 siRNA was co-delivered with DOX in the multifunctional micelles. The nuclear distribution of DOX observed by integrated micelles containing mdr1 siRNA led to the sensitization of MDA-MB-435/LCC6MDR1-resistant cells to DOX (Figure 5B). Consistent with previous observations, the level of resistance reversal was the highest for micelles containing dual functionalities on the micellar shell.

In further studies, traceable micellar formulations for integrated DOX and siRNA delivery were developed to track the fate of the nanodelivery system and its incorporated cargo *in vivo*. The ability to track the *in vivo* behavior of the nanodelivery offers the possibility for image-guided drug delivery and monitoring of cancer response to the treatment by noninvasive methods. There has been considerable interest in the development of nanotechnology platforms to image and treat cancers by using targeted delivery and controlled drug release in recent years. For example, Feng *et al.* developed an immunoliposome system modified by the fusion peptide of antiepidermal growth factor receptor (EGFR) monoclonal antibody for *in vivo* drug delivery and imaging.[30] A magnetic nanoparticle-based delivery system with dual-purpose probes was developed for *in vivo* transfer of siRNA and the simultaneous imaging of its accumulation in tumors by high-resolution MRI and NIRF.[31] NIFR probes such as Cy5.5 and Dy677 enable deep tissue imaging with high penetration and low tissue absorption and scattering, representing an ideal noninvasive technology for *in vivo* imaging. A comparison of *in vivo* images of the biodistribution of NON-micelles and RGD-micelles clearly showed the effect of RGD modification in enhancing micellar tumor accumulation (Figure 6B). Unlike chemically conjugated DOX, the complexed siRNA might dissociate from micelles or be degraded during circulation after systemic administration. The observation of Dy677 fluorescence in tumors indicated that RGD-micelles can protect siRNA during circulation and deliver siRNA into the tumor tissue (Figure 6C), pointing to the potential of this nanomedicine platform for siRNA-based cancer therapy. The particular bright fluorescence in the liver and kidney reflected the RES accumulation of these micelles, which may cause the rapid elimination of micelles from the body, leading to relatively low or failed tumor accumulation for NON-micelles (Figure 6B and C). The ongoing study in our lab is aimed at assessing the therapeutic efficacy of RGD/TAT-micelles containing DOX and mdr1-siRNA for the treatment of MDR tumors.

CONCLUSIONS

In this study, we have reported the design, synthesis, and evaluation of the PEO-*b*-polyester-based micellar nanomedicine for traceable co-delivery of siRNA and DOX. The prepared micelles have a versatile core that can stably complex siRNA and conjugate DOX and imaging probes and have a virus-like shell for cell-specific recognition and efficient cellular uptake. We demonstrated that these micelles could release intact DOX by a pH-triggered mechanism. The peptide-functionalized micelles, especially RGD/TAT-micelles

containing mdr1-siRNA and DOX, demonstrated significant cellular uptake, improved DOX penetration into nuclei, and finally enhanced DOX cytotoxicity in these DOX-resistant cells. Incorporation of fluorescent probes in the micellar core allows for *in vitro* and *in vivo* tracking of micelles. Although preliminary, the results of this study demonstrated a tremendous potential of this multifunctional micellar nanomedicine for efficient delivery of anticancer drugs and oncogene-silencing siRNA to their cellular and molecular targets.

MATERIALS AND METHODS

Materials. The scrambled siRNAs (Silencer Negative siRNA and Silencer FAM-labeled Negative siRNA) and the anti-mdr1 siRNA (mdr1-siRNA) were purchased from Ambion (Austin, TX). Dy677-siRNA was purchased from Dharmacon Inc. (Lafayette, LA). Cy5.5 monofunctional dye was purchased from GE Healthcare (Piscataway, NJ). Cell culture media RPMI 1640, penicillin–streptomycin, fetal bovine serum, L-glutamine, and HEPES buffer solution (1 M) were purchased from GIBCO, Invitrogen Corp (Carlsbad, CA). RGD4C (KACDCRGDCFCG, MW 1273.9), cyclic RGDfK (cRGDfK), and TAT peptide (CGRKKRRQRRR) were purchased from Anaspec Inc. (Torrence, CA). Doxorubicin (DOX) was purchased from Hisun Pharmaceutical Co (Zhejiang, China). All other chemicals were reagent grade.

Polymer Synthesis. Acetal-PEO-*b*-PCCL was synthesized as previously reported.[32] Acetal-PEO-*b*-P(CL-Hyd-DOX), acetal-PEO-*b*-P(CL-g-SP), and acetal-PEO-*b*-P(CL-g-DP) were synthesized from acetal-PEO-*b*-PCCL as previously reported.[27,32] RGD4C-attached PEO-*b*-P(CL-Hyd-DOX) and RGD4C-attached PEO-*b*-P(CL-g-DP) were synthesized from acetal-PEO-*b*-PCCL according to the method with a slight modification.[26,32] RGD4Cwas conjugated to the micelles at an RGD4C:polymer molar ratio of 1:5. The conjugation efficiency of RGD4C peptide to polymeric micelles was determined by a reverse gradient HPLC method as previously reported.[26] The resulting polymer solution was dialyzed against distilled water and lyophilized.

Conjugation of TAT to the PEO terminus of acetal-PEO-*b*-P(CL-g-SP) was performed using thiazolidine ring formation.[33] To do this, a micellar solution of acetal-PEO-*b*-P(CL-g-SP) (24 mg, 3.6 μmol) in 8 mL of 0.2 M acetate buffer (AcOH) (pH 4.0) was prepared and incubated with TAT (3 mg, 2 μmol) with stirring for 5 days. The conjugation efficiency of TAT peptide to polymeric micelles was determined by a reverse gradient HPLC method as previously reported.[28] The resulting polymer solution was dialyzed against distilled water and lyophilized to obtain TAT-PEO-*b*-P(CL-g-SP).

For *in vivo* imaging studies, NIRF Cy5.5. was conjugated to acetal-PEO-*b*-P(CL-g-SP) by addition of an acetal-PEO-*b*-P(CL-g-SP) solution (20 mg/mL) (pH adjusted to 9.6 with 0.5 M sodium bicarbonate) to 1 mg of Cy5.5 monofunctional reactive dye, followed by incubation with stirring at room temperature in the dark for 1 h. After incubation, the mixture was separated from the nonreacted dye by dialysis against distilled water followed by lyophilization. The Cy5.5 conjugation efficiency was determined by a UV/vis spectrophotometer, measuring the extinction coefficient of Cy5.5 at 675 nm (2.5×10^5 M^{-1} cm^{-1}) as described by the manufacturer.

Micelle Preparation and Characterization of Micelles for Co-delivery of siRNA and DOX. The copolymers, *i.e.*, acetal-PEO-*b*-P(CL-g-SP), TAT-PEO-*b*-P(CL-g-SP), acetal-PEO-*b*-P(CL-Hyd-DOX), and RGD-4C-PEO-*b*-P(CL-Hyd-DOX), were used to prepare micelles containing complexed siRNA and conjugated DOX. The polymer compositions of acetal-PEO-*b*-P(CL-g-SP)/acetal-PEO-*b*-P(CL-Hyd-DOX) (2:4, weight ratio), acetal-PEO-*b*-P(CL-g-SP)/RGD4C-PEO-*b*-P(CL-Hyd-DOX) (2:4, weight ratio), acetal-PEO-*b*-P(CL-g-SP)/TAT-PEO-*b*-P(CL-g-SP)/acetal-PEO-*b*-P(CL-Hyd-DOX) (1:1:4, weight ratio), and acetal-PEO-*b*-P(CL-g-SP)/TAT-PEO-*b*-P(CL-*g*-SP)/RGD-PEO-*b*-P(CL-Hyd- DOX) (1:1:4, weight ratio) were used to prepare nontargeted micelles (NON-micelles), RGD-modified micelles (RGD-micelles), TAT-modified micelles (TAT-micelles), and RGD/TAT-modified micelles (RGD/TAT-micelles), respectively (Table 1). To avoid siRNA binding to the positively charged TAT or RGD on the micellar shell, acetal-PEO-*b*-P(CL-g-SP) was first used to complex siRNA by incubating siRNA with acetal-PEO-*b*-P(CL-g-SP) (1:8 weight ratio, siRNA to polymer) in HEPES buffer solution (pH 6.5) at 37 °C for 10 min. Then RGD4C-PEO-*b*-P(CL-Hyd-DOX), TAT-PEO-*b*-P(CL-g-SP), or both of them were added to the resulting polymer/siRNA complex and incubated at 37 °C for 30 min to prepare shell-functionalized micelles containing DOX and siRNA in the core. The final ratio of siRNA to polycationic copolymer in all the micellar formulations was fixed at 1:16 (weight ratio).

For the preparation of Cy5.5-labeled NON- and RGD-micelles (NON- and RGD-micelles-DOX-Cy5.5) for *in vivo* imaging study, acetal-PEO-*b*-P(CL-g-SP-Cy5.5) was used to replace acetal-PEO-*b*-P(CL-g-SP) in NON- or RGD-micelles. A separate set of samples was also prepared using acetal- and RGD4C-PEO-*b*-P(CL-g-DP) to replace acetal- and RGD4C-PEO-*b*-P(CL-Hyd-DOX), respectively, to prepare NON- and RGD-micelles containing complexed Dy677-siRNA (NON- and RGD-micelles/Dy677-siRNA).

The particle size of the micelles was determined by a dynamic light scattering (DLS) spectrometer (Malvern Zetasizer 3000, UK). The micelles were visualized by atomic force microscopy (AFM) after overnight air drying of a micellar solution on a clean mica surface, using a Molecular Force Probe 3D (MFP 3D) from Asylum Research (Santa Barbara, CA) controlled with IGOR PRO software (Wavemetrics, Portland, OR). To investigate pH-triggered DOX release, acetal-micelles were incubated in PBS (pH 7.2) or acetate buffer (pH 5.0) for 48 h. At different points, the DOX emission spectrum for the micellar solution was scanned by a fluorescence spectrophotometer excited at 485 nm.

siRNA Binding by Gel Retardation Assay. The siRNA binding ability of the NON-micelles composed of acetal-PEO-*b*-P(CL-Hyd-DOX)/acetal-PEO-*b*-P(CL-g-SP) was analyzed by agarose gel electrophoresis. NON-micelles/siRNA complexes were prepared by mixing 8 μL of 0.1 M HEPES buffer (pH 6.5) with 4 μL of negative control siRNA (containing 2 μg of siRNA) and 8 μL of serially diluted concentrations of a acetal-PEO-*b*-P(CL-g-SP) solution (containing polymers ranging from 2 μg to 16 μg) and incubated for 30 min at 37 °C, after which 4 μL of 6× sample buffer (50% glycerol, 1% bromophenol blue, and 1% cylene cyenol FF in TBE buffer) was added, and the samples were loaded onto 2% agarose gels containing 0.05 mg/mL ethidium bromide. Electrophoresis was performed at 130 mV and ~52 mA for 15 min. The resulting gels were photographed under UV illumination. The pictures were digitized and analyzed with Scion Image Analysis software to determine the mean density of siRNA bands. The binding percentage was calculated on the basis of the relative intensity of the free siRNA band in each well, compared to wells with free siRNA (*i.e.*, in the absence of any polymers).

Cell Lines and Animal Models. The P-gp-overexpressing human melanoma cell line MDA-MB-435/LCC6MDR1 was kindly provided by Dr. Robert Clarke (Georgetown University Medical School, Washington, DC).[34,35] Cell culture media RPMI 1640, penicillin–streptomycin, fetal bovine serum, L-glutamine, and HEPES buffer solution (1 M) were purchased from GIBCO, Invitrogen Corp. Cells were grown and maintained in RPMI 1640 supplemented with 10% fetal bovine serum at 37 °C and 5% CO_2. Cells were used in exponential growth phase, for up to a maximum of 20 *in vitro* passages.

Female athymic nude mice (NCRNU-F) were purchased from Taconic Farms Inc. All the animals were kept in standard housing. All animal studies were conducted in accordance with the Canadian Council on Animal Care Guidelines and Policies with approval from the Animal Care and Use Committee for the University of Alberta (Edmonton, AB, Canada). To establish the tumor model, mice were inoculated with 2×10^6 MDA-MB-435/LCC6MDR1 cells in a volume of 100 μL of PBS injected sc in the right rear flank. The mice were used when the tumors reached a size of about 0.1 cm^3 (14 days after transplantation).

Flow Cytometry Analysis. Two-color flow cytometry was used to characterize the micelles co-encapsulating DOX and FAM-siRNA or to determine the cellular uptake of FAM-siRNA and DOX formulated in micelles. To determine the cellular uptake, cells were seeded into 12-well plates and incubated at 37 °C until 70% confluence was reached. Micelles containing conjugated DOX (5 μg/mL equivalent DOX) and FAM-siRNA (100 nM) were added and incubated for 1 h at 37 °C. The medium was aspirated, and cells were rinsed three times with cold PBS. The cells were then trypsinized, washed with cold PBS, filtered through 35 μm nylon mesh, and finally examined on a FACsort flow cytometer (Becton-Dickinson Instruments, Franklin Lakes, NJ). For the competitive inhibition study, MDA-MB-435/LCC6MDR1 were first preincubated with free cRGDfK peptides (5 mM) for 30 min and then incubated with RGD/TAT-micelles. Flow cytometry and sorting were performed on a FACS using a 488 nm argon laser and FL1 band-pass emission for the green FAM-siRNA (530 ± 20) or FL3 band-pass emission (610 ± 10) for the red DOX. Fluorescence histograms and dot plots were generated using Cell Quest software (for figures, histograms were recreated using FASexpress software).

Confocal Microscopy Study. A laser confocal scanning microscope was used to evaluate the cellular uptake and intracellular distribution of micelles incubated with MDA-MB-435/LCC6-MDR1 cells. Resistant cells were grown on coverslips to 50% confluence and incubated with various DOX formulations (containing 5 μg equivalent/mL DOX and 100 nM siRNA) diluted in culture medium at 37 °C. To evaluate the cellular uptake, the cells were incubated with the micellar formulations for 1 h, washed three times with PBS, fixed in paraformaldehyde in PBS for 10 min, and then treated with DAPI (excitation/emission: 345/661 nm) for 15 min to stain nuclei. To observe the intracellular distribution of micelles, cells were incubated with micellar formulations for 4 h. At the end of incubation, LysoTracker Green, Blue, or Red (50 nM, Molecular Probes, Invitrogen Co., OR) was added and incubated with the cells for 0.5 h for endosome/lysosome labeling. The cells were imaged by a Zeiss 510 LSMNLO confocal microscope (Carl Zeiss Microscope Systems, Jena, Germany) with identical settings for each confocal study.

***In Vitro* Cytotoxicity.** Cytotoxicity of micelles with co-delivered mdr1 siRNA and DOX against MDA-MB-435/LCC6MDR1 cells was evaluated using the 3-(4,5-dimethylthiazol-2-yl)-2,5-diphenyltetrazolium bromide (MTT) assay. Growth medium RPMI-1640 (100 μL) containing 4000 cells was placed in each well in 96-well plates and incubated overnight to allow cell attachment. Cells were then exposed to different formulations containing 100 nM mdr1 siRNA and 5 μg DOX equivalent/mL at 37 °C for 72 h, followed by the addition of 20 μL of MTT solution (5 mg/mL). Three hours later, medium was removed and replaced with 200 μL of DMSO. Cell viability compared to control wells of untreated cells was determined by measuring the optical absorbance differences between 570 and 650 nm using a PowerwaveX340 microplate reader (BIO-TEK Instruments, Inc., Nepean, Ontario, Canada).

***In Vivo* Optical Imaging.** For optical imaging, NON- and RGD-micelles-DOX-Cy5.5, with an equivalent of 1.25 mg/kg DOX, or NON- and RGD-micelles/Dy647-siRNA with an equivalent of 100 nmol/kg siRNA, were intravenously injected into tumor-bearing mice. Mice were then anesthetized and placed into a whole-body animal imaging system (Imaging Station IS4000-MM, Kodak), equipped with band-pass excitation and long-pass emission filters at 630 and 700 nm for near-infrared fluorescent imaging (Chroma Technology Corporation, Rockingham, VT). *In vivo* imaging was performed 24 h after injection of micellar formulations. Exposure time was 30 s per image for NIRF image and 1 s for visible image.

Acknowledgment. This research was funded by research grants from the Alberta Cancer Foundation (ACF) and Canadian Institutes of Health Research (CIHR). We thank Ms. Elaine Moase for her technical support in animal experiments as well as editorial reviewing of this paper. We also thank Dr Kamaljit Kaur for the use of Imaging Station IS4000-752 MM, Kodak.

REFERENCES AND NOTES

1. Allen, T. M.; Cullis, P. R. Drug Delivery Systems: Entering the Mainstream. *Science* **2004**, *303*, 1818–1822.
2. Langer, R. Drug Delivery and Targeting. *Nature* **1998**, *392*, 5–10.
3. Maeda, H.; Wu, J.; Sawa, T.; Matsumura, Y.; Hori, K. Tumor Vascular Permeability and the EPR Effect in Macromolecular Therapeutics: A Review. *J. Controlled Release* **2000**, *65*, 271–284.
4. Iyer, A. K.; Khaled, G.; Fang, J.; Maeda, H. Exploiting the Enhanced Permeability and Retention Effect for Tumor Targeting. *Drug Discovery Today* **2006**, *11*, 812–818.
5. Brannon-Peppas, L.; Blanchette, J. O. Nanoparticle and Targeted Systems for Cancer Therapy. *Adv. Drug. Delivery Rev.* **2004**, *56*, 1649–1659.
6. Riordan, J. R.; Deuchars, K.; Kartner, N.; Alon, N.; Trent, J.; Ling, V. Amplification of P-glycoprotein Genes in Multidrug-resistant Mammalian-cell Lines. *Nature* **1985**, *316*, 817–819.
7. Ueda, K.; Cardarelli, C.; Gottesman, M. M.; Pastan, I. Expression of a Full-length cDNA for the Human "mdr1" Gene Confers Resistance to Colchicine, Doxorubicin, and Vinblastine. *Proc. Natl. Acad. Sci. U. S. A.* **1987**, *84*, 3004–3008.
8. Shukla, S.; Wu, C. P.; Ambudkar, S. V. Development of Inhibitors of ATP-binding Cassette Drug Transporters: Present Status and Challenges. *Expert Opin. Drug Metab. Toxicol.* **2008**, *4*, 205–223.
9. Ferry, D. R.; Traunecker, H.; Kerr, D. J. Clinical Trials of P-glycoprotein Reversal in Solid Tumours. *Eur. J. Cancer* **1996**, *32A*, 1070–1081.
10. Lage, H. MDR1/P-glycoprotein (ABCB1) as Target for RNA Interference-mediated Reversal of Multidrug Resistance. *Curr. Drug Targets* **2006**, *7*, 813–821.
11. Stierle, V.; Laigle, A.; Jolles, B. Modulation of MDR1 Gene Expression in Multidrug Resistant MCF7 Cells by Low Concentrations of Small Interfering RNAs. *Biochem. Pharmacol.* **2005**, *70*, 1424–1430.
12. Wu, H.; Hait, W. N.; Yang, J. M. Small Interfering RNA-Induced Suppression of MDR1 (P-glycoprotein) Restores Sensitivity to Multidrug-resistant Cancer Cells. *Cancer Res.* **2003**, *63*, 1515–1519.
13. Patil, Y. B.; Swaminathan, S. K.; Sadhukha, T.; Ma, L. A.; Panyam, J. The Use of Nanoparticle-mediated Targeted Gene Silencing and Drug Delivery to Overcome Tumor Drug Resistance. *Biomaterials* **2010**, *31*, 358–365.
14. Wang, Y.; Gao, S. J.; Ye, W. H.; Yoon, H. S.; Yang, Y. Y. Co-delivery of Drugs and DNA from Cationic Core-shell Nanoparticles Self-assembled from a Biodegradable Co-polymer. *Nat. Mater.* **2006**, *5*, 791–796.
15. Chen, Y.; Bathula, S. R.; Li, J.; Huang, L. Multi-functional Nanoparticles Delivering siRNA and Doxorubicin Overcome Drug Resistance in Cancer. *J. Biol. Chem.* **2010**, *285*, 22639−22850.
16. Chen, A. M.; Zhang, M.; Wei, D.; Stueber, D.; Taratula, O.; Minko, T.; He, H. Co-Delivery of Doxorubicin and Bcl-2 Sirna by Mesoporous Silica Nanoparticles Enhances the Efficacy of Chemotherapy in Multidrug-Resistant Cancer Cells. *Small* **2009**, *5*, 2673–2677.
17. Dong, X.; Liu, A.; Zer, C.; Feng, J.; Zhen, Z.; Yang, M.; Zhong, L. siRNA Inhibition of Telomerase Enhances the Anticancer Effect of Doxorubicin in Breast Cancer Cells. *BMC Cancer* **2009**, *9*, 133.
18. Liu, W. L.; Green, N.; Seymour, L. W.; Stevenson, M. Paclitaxel Combined with siRNA Targeting HPV16 Oncogenes

Improves Cytotoxicity for Cervical Carcinoma. *Cancer Gene. Ther.* **2009**, *16*, 764–775.
19. Park, S. Y.; Lee, W.; Lee, J.; Kim, I. S. Combination Gene Therapy Using Multidrug Resistance (MDR1) Gene shRNA and Herpes Simplex Virus-thymidine Kinase. *Cancer Lett.* **2008**, *261*, 205–214.
20. Lima, R. T.; Martins, L. M.; Guimaraes, J. E.; Sambade, C.; Vasconcelos, M. H. Specific Downregulation of bcl-2 and xIAP by RNAi Enhances the Effects of Chemotherapeutic Agents in MCF-7 Human Breast Cancer Cells. *Cancer Gene Ther.* **2004**, *11*, 309–316.
21. Karagiannis, E. D.; Anderson, D. G. Minicells Overcome Tumor Drug-Resistance. *Nat. Biotechnol.* **2009**, *27*, 620–621.
22. Zhu, C. H.; Jung, S.; Luo, S. B.; Meng, F. H.; Zhu, X. L.; Park, T. G.; Zhong, Z. Y. Co-delivery of siRNA and Paclitaxel into Cancer Cells by Biodegradable Cationic Micelles Based on PDMAEMA-PCL-PDMAEMA Triblock Copolymers. *Biomaterials* **2010**, *31*, 2408–2416.
23. Nasongkla, N.; Bey, E.; Ren, J. M.; Ai, H.; Khemtong, C.; Guthi, J. S.; Chin, S. F.; Sherry, A. D.; Boothman, D. A.; Gao, J. M. Multifunctional Polymeric Micelles as Cancer-targeted, MRI-ultrasensitive Drug Delivery Systems. *Nano Lett.* **2006**, *6*, 2427–2430.
24. Guthi, J. S.; Yang, S. G.; Huang, G.; Li, S.; Khemtong, C.; Kessinger, C. W.; Peyton, M.; Minna, J. D.; Brown, K. C.; Gao, J. MRI-visible Micellar Nanomedicine for Targeted Drug Delivery to Lung Cancer Cells. *Mol. Pharmaceutics* **2010**, *7*, 32–40.
25. Hong, G. B.; Yuan, R. X.; Liang, B. L.; Shen, J.; Yang, X. Q.; Shuai, X. T. Folate Functionalized Polymeric Micelle as Hepatic Carcinoma-targeted, MRI-ultrasensitive Delivery System of Antitumor Drugs. *Biomed. Microdevices* **2008**, *10*, 693–700.
26. Xiong, X. B.; Ma, Z. S.; Lai, R.; Lavasanifar, A. The Therapeutic Response to Multifunctional Polymeric Nano-conjugates in the Targeted Cellular and Subcellular Delivery of Doxorubicin. *Biomaterials* **2010**, *31*, 757–768.
27. Xiong, X. B.; Uludag, H.; Lavasanifar, A. Biodegradable Amphiphilic Poly(ethylene oxide)-block-Polyesters with Grafted Polyamines as Supramolecular Nanocarriers for Efficient siRNA Delivery. *Biomaterials* **2009**, *30*, 242–253.
28. Xiong, X. B.; Uludag, H.; Lavasanifar, A. Virus-mimetic Polymeric Micelles for Targeted siRNA Delivery. *Biomaterials* **2010**, *31*, 5886–5893.
29. Meng, H. A.; Liong, M.; Xia, T. A.; Li, Z. X.; Ji, Z. X.; Zink, J. I.; Nel, A. E. Engineered Design of Mesoporous Silica Nanoparticles to Deliver Doxorubicin and P-glycoprotein siRNA to Overcome Drug Resistance in a Cancer Cell Line. *ACS Nano* **2010**, *4*, 4539–4550.
30. Feng, B.; Tomizawa, K.; Michiue, H.; Han, X. J.; Miyatake, S.; Matsui, H. Development of a Bifunctional Immunoliposome System for Combined Drug Delivery and Imaging in Vivo. *Biomaterials* **2010**, *31*, 4139–4145.
31. Medarova, Z.; Pham, W.; Farrar, C.; Petkova, V.; Moore, A. *In vivo* Imaging of siRNA Delivery and Silencing in Tumors. *Nat. Med.* **2007**, *13*, 372–377.
32. Xiong, X. B.; Mahmud, A.; Uludag, H.; Lavasanifar, A. Multifunctional Polymeric Micelles for Enhanced Intracellular Delivery of Doxorubicin to Metastatic Cancer Cells. *Pharm. Res.* **2008**, *25*, 2555–2566.
33. Oba, M.; Fukushima, S.; Kanayama, N.; Aoyagi, K.; Nishiyama, N.; Koyama, H.; Kataoka, K. Cyclic RGD Peptide-conjugated Polyplex Micelles as a Targetable Gene Delivery System Directed to Cells Possessing Alpha(v)beta(3) and Alpha(v)beta(5) Integrins. *Bioconjugate Chem.* **2007**, *18*, 1415–1423.
34. Leonessa, F.; Green, D.; Licht, T.; Wright, A.; Wingate-Legette, K.; Lippman, J.; Gottesman, M. M.; Clarke, R. MDA435/LCC6 and MDA435/LCC6MDR1: Ascites Models of Human Breast Cancer. *Br. J. Cancer* **1996**, *73*, 154–161.
35. Wong, H. L.; Bendayan, R.; Rauth, A. M.; Xue, H. Y.; Babakhanian, K.; Wu, X. Y. A Mechanistic Study of Enhanced Doxorubicin Uptake and Retention in Multidrug Resistant Breast Cancer Cells Using a Polymer-lipid Hybrid Nanoparticle System. *J. Pharmacol. Exp. Ther.* **2006**, *317*, 1372–1381.